


Article

Gd₂O₃ Doped UO₂(s) Corrosion in the Presence of Silicate and Calcium under Alkaline Conditions

Sonia García-Gómez ^{1,*} , Javier Giménez ¹ , Ignasi Casas ¹, Jordi Llorca ¹  and Joan De Pablo ^{1,2}

¹ Department of Chemical Engineering, EEBE and Barcelona Research Center in Multiscale Science and Engineering, Universitat Politècnica de Catalunya (UPC), Eduard Maristany, 10-14, 08019 Barcelona, Spain; francisco.javier.gimenez@upc.edu (J.G.); ignasi.casas@upc.edu (I.C.); jordi.llerca@upc.edu (J.L.); joan.de.pablo@upc.edu (J.D.P.)

² EURECAT, Centre Tecnològic de Catalunya, Plaça de la Ciència 2, 08243 Manresa, Spain

* Correspondence: sonia.garcia.gomez@upc.edu

Abstract: The anodic reactivity of UO₂ and UO₂ doped with Gd₂O₃ was investigated by electrochemical methods in slightly alkaline conditions in the presence of silicate and calcium. At the end of the experiments, the electrodes were analysed by X-ray photoelectron spectroscopy to determine the oxidation state of the uranium on the surface. The experiments showed that the increase in gadolinia doping level led to a reduction in the reactivity of UO₂, this effect being more marked at the highest doping level studied (10 wt.% Gd₂O₃). This behaviour could be attributed to the formation of dopant-vacancy clusters (Gd^{III}-Ov), which could limit the accommodation of excess O²⁻ into the UO₂ lattice. In addition, the presence of Ca²⁺ and SiO₃²⁻ decreased the anodic dissolution of UO₂. In summary, the Gd₂O₃ doping in presence of silicate and calcium was found to strongly decrease the oxidative dissolution of UO₂, which is a beneficial situation regarding the long-term management of spent nuclear fuel in a repository.

Keywords: UO₂(s); gadolinia doping; anodic oxidation; X-ray photoelectron spectroscopy; silicate and calcium ions



Citation: García-Gómez, S.; Giménez, J.; Casas, I.; Llorca, J.; De Pablo, J. Gd₂O₃ Doped UO₂(s) Corrosion in the Presence of Silicate and Calcium under Alkaline Conditions. *Inorganics* **2023**, *11*, 469. <https://doi.org/10.3390/inorganics11120469>

Academic Editors: Roberto Nisticò, Torben R. Jensen and Luciano Carlos

Received: 7 October 2023

Revised: 25 November 2023

Accepted: 29 November 2023

Published: 1 December 2023



Copyright: © 2023 by the authors. Licensee MDPI, Basel, Switzerland. This article is an open access article distributed under the terms and conditions of the Creative Commons Attribution (CC BY) license (<https://creativecommons.org/licenses/by/4.0/>).

1. Introduction

The repository concept is an internationally accepted approach for the long-term management of spent nuclear fuel, where the fuel would be sealed in containers. However, in the worst-case-scenario where the containers fail, the contact of the fuel with groundwater could be possible. Since the majority of the radionuclides are located within the UO₂ matrix and taking into account that U^{VI} is more soluble than U^{IV}, the release of the radionuclides to the groundwater would be controlled by the fuel corrosion/dissolution rate, which would be strongly affected by the redox conditions. Under oxidizing aqueous conditions, the corrosion of UO₂ occurs via two steps process. First U^{IV}O₂ is oxidized to U^{IV}_{1-2x}U^V_{2x}O_{2+x} forming a thin oxidized surface layer, while in the second step soluble U^{VI} is released to the solution [1]. In alkaline conditions, dissolved uranium could reprecipitate, forming corrosion product deposits (UO₃·yH₂O).

Some of the main parameters affecting the corrosion of the UO₂ matrix in a repository are the rare earth (RE) doping of the fuel [2,3] and the composition of the groundwater [4]. Nowadays, UO₂ is commonly doped with rare earth elements such as Gd (in the form of Gd₂O₃) [5] for its critical role as a burnable neutron absorber. The high neutron absorption cross section of ¹⁵⁵Gd and ¹⁵⁷Gd helps to counterbalance the excess of reactivity in the reactor core during the initial stages of operation, improving overall reactor performance.

The influence of the incorporation of Gd to UO₂ has been extensively studied to determine lattice parameters [6,7], UO₂ oxidation in dry experiments [8,9], UO₂ electrochemical reactivity [1,7,10] and UO₂ dissolution [11,12].

Air oxidation kinetics of UO_2 at high temperature (325 °C) indicated that doping with Gd stabilizes the first oxidation product and inhibits the oxidation to U_3O_8 being the kinetic mechanism dependent on the Gd content [8]. He et al. studied the effect of fission product doping on the anodic reactivity of UO_2 (they worked with SIMFUEL) and concluded that doping with such elements distorts the lattice structure of UO_2 . This fact affects its corrosion process, since the oxidation was suppressed as the extent of doping increased [1]. Liu et al. showed that Gd doping lead to a contraction of the fluorite lattice, reducing the electrochemical reactivity of $(\text{U}_{1-y}\text{Gd}_y)\text{O}_2$ [7]. Razdan and Shoemith studied the influence of trivalent-dopants (such as Gd^{III}) on the electrochemical behaviour of UO_2 [2]. They found that while the mechanism of oxidation/dissolution of Gd-doped UO_2 is comparable to that of SIMFUEL, the reactivity is lower. The effect of Gd-doping was also observed on dissolution experiments, showing a reduction of the oxidative dissolution rate [11–13]. This behaviour was commonly attributed to the formation of $\text{Gd}^{\text{III}}\text{-O}_v$ clusters [14] in order to maintain electroneutrality, limiting the accommodation of O^{2-} ions during oxidation [15]. Therefore, the Gd^{III} influence on fuel reactivity under repository conditions is of great importance.

Concrete has been proposed as a construction material in some deep geological repositories [16]. Water in contact with concrete presents high pH values and contains silicate and calcium ions [17]. Flow-through dissolution experiments with UO_2 performed by Wilson and Gray [4] revealed a considerable reduction in the concentration of U measured when Ca and Si were present in the solution. Santos et al. investigated the effect of SiO_3^{2-} [18] and Ca^{2+} on the corrosion of SIMFUEL [19]. The authors concluded that these ions had little influence on the first oxidation step, but they inhibited/retarded the formation of U^{VI} , probably due to the adsorption of silicate and calcium on the fuel surface. Espriu et al. studied the corrosion of SIMFUEL at high pH and in the presence of calcium and silicate [20]. Their X-ray photoelectron spectroscopy (XPS) analysis evidenced that the presence of both ions in a high alkaline solution have a significant impact on the oxidation of the surface of SIMFUEL, since the surface was less oxidized than that of the experiments conducted in a solution without such ions. However, the corrosion of Gd_2O_3 doped UO_2 under cementitious water is not well known.

In this work, both undoped UO_2 and UO_2 doped with 5 and 10 wt.% Gd_2O_3 pellets were examined electrochemically in order to study the influence of Gd_2O_3 doping on the oxidative reactivity of UO_2 at slightly alkaline groundwater in the presence of silicate and calcium.

2. Results and Discussion

2.1. Characterisation of the Gd_2O_3 Doped UO_2 Pellets

The surface morphology of the sintered UO_2 pellets doped with 5 wt.% and 10 wt.% Gd_2O_3 (Figure 1), exhibited clearly defined grain boundaries and low-porosity microstructure. Furthermore, no unreacted Gd_2O_3 was found and EDX analysis revealed a homogeneous distribution of gadolinium within the UO_2 matrix.

The examination of the samples using X-ray diffraction (XRD) revealed the fluorite crystal structure of UO_2 (Figure 2). The peaks observed in the Gd_2O_3 -doped samples were found to be slightly shifted toward greater angles compared to the UO_2 sample. This shift was caused by the lattice contraction as gadolinium concentration increased, as previously observed in previous studies [7].

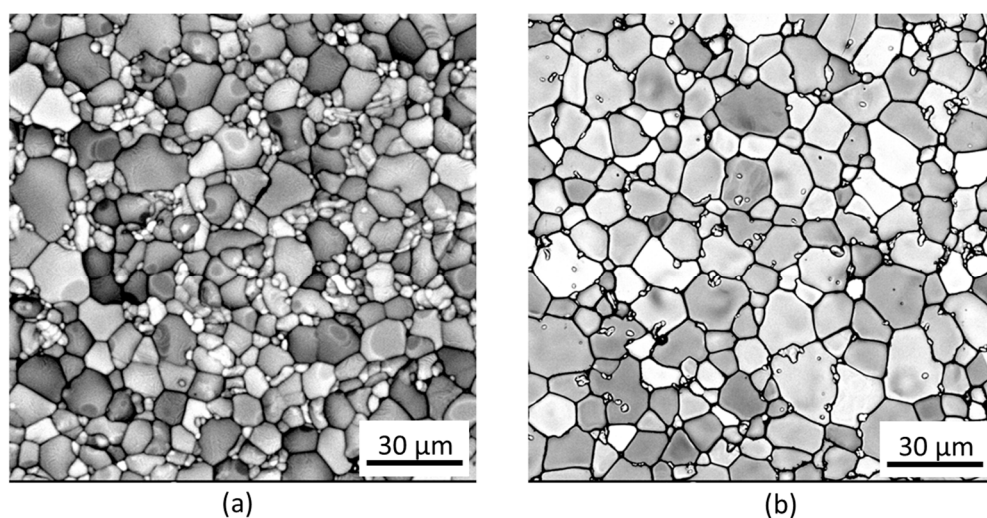


Figure 1. Scanning electron micrograph of UO_2 doped with 5 wt.% Gd_2O_3 (a) and 10 wt.% (b) Gd_2O_3 after sintering.

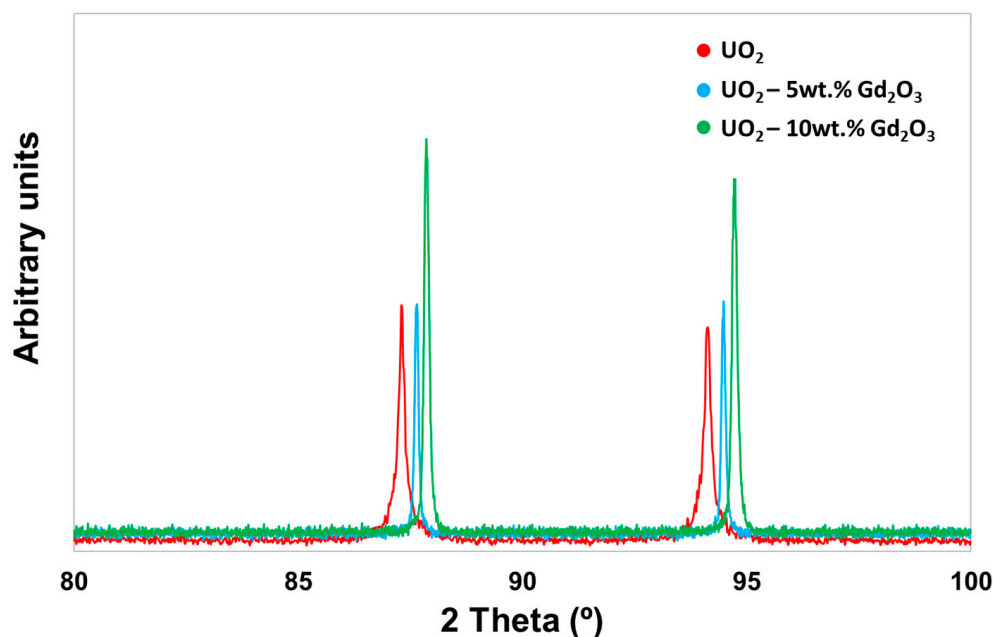


Figure 2. Close-up of the XRD spectra of non-doped UO_2 and UO_2 doped with 5 wt.% and 10 wt.% Gd_2O_3 .

2.2. Cyclic Voltammetry

Figure 3 shows a series of cyclic voltammograms (CVs) recorded in silicate and calcium solution on the undoped and Gd_2O_3 doped UO_2 electrodes. Similar stages of both oxidation and reduction regions were previously observed for SIMFUEL [21] and undoped UO_2 [22]. In the forward scan, two different regions can be observed. In region 1 (at the potential of around -0.2 V), the increase in the anodic oxidation current observed is attributed to the formation of a mixed $\text{U}^{\text{IV}}/\text{U}^{\text{V}}$ thin surface oxide layer with a thickness limited by the O^{2-} injection into the UO_2 fluorite lattice. It can be observed that the onset of the oxidation in region 1 is independent of the Gd_2O_3 doping level. However, there is a significant difference in the anodic current observed, registering lower current density values as the doping level of Gd_2O_3 increases. This behaviour was observed in [10] for hyperstoichiometric $\text{U}_{1-y}\text{Gd}_y\text{O}_{2+x}$ and can be attributed to the ability of Gd to retard the oxidation of UO_2 matrix surface by the formation of $\text{Gd}^{\text{III}}\text{-Ov}$ clusters. In region 2 (>0.2 V),

the thin surface layer is further oxidized to soluble U^{VI} and then the dissolution as UO_2^{2+} could take place. Under alkaline conditions, the solubility of UO_2^{2+} is limited [1], therefore it could be deposited as insoluble $U^{VI}O_3 \cdot yH_2O$ on the electrode surface. The formation of this deposit could explain the suppression of the current observed in Figure 3 at higher voltages (>0.3 V). Another possibility is that the silicate and calcium in solution could be adsorbed on the electrode surface, suppressing the further oxidation of the thin surface layer [19]. The stabilization of the UO_2 matrix in presence of silicate and calcium was previously observed on SIMFUEL [18–20].

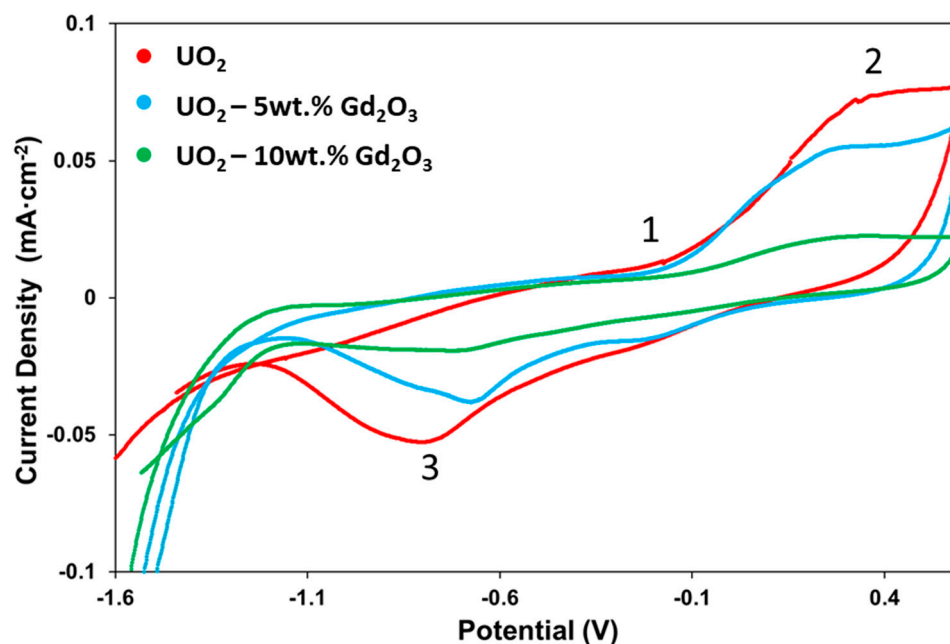


Figure 3. CVs recorded on the three different electrodes (rotation rate of 1000 rpm) in a solution that contains 0.1 M NaCl, 10^{-2} M SiO_3^{2-} and 10^{-3} M Ca^{2+} , pH = 10, at a scan rate of $10 \text{ mV} \cdot \text{s}^{-1}$. The potential was scanned from -1.6 V to 0.6 V and back.

On the reverse scan, a cathodic reduction peak (region 3) was observed with a maximum at around -0.7 V. This reduction peak is commonly attributed to the reduction of $U^{IV}_{1-2x}/U^{V}_{2x}O_{2+x}/U^{VI}O_3 \cdot yH_2O$ surface layer [2]. The presence of this reduction peak for all electrodes indicate that an oxidized surface layer is formed despite the presence of Gd, however, the current associated with the reduction peak vary significantly with doping level. This confirms that the thickness of the thin $U^{IV}_{1-2x}/U^{V}_{2x}O_{2+x}$ layer differs among them, which is in agreement with the current densities registered in regions 1 and 2.

In contrast, CV experiments performed on 5 wt.% Gd_2O_3 -doped UO_2 electrode in presence of bicarbonate (Figure 4) registered higher anodic oxidation currents in regions 1 and 2 than in solutions that contained silicate and calcium. This behaviour can be attributed to the ability of bicarbonate to form soluble uranyl carbonate complex ions, which avoided the formation of secondary phases on the electrode surface and enhanced the oxidation and dissolution process of UO_2 [23]. This is consistent with the smaller reduction peak observed in region 3 in bicarbonate solution.

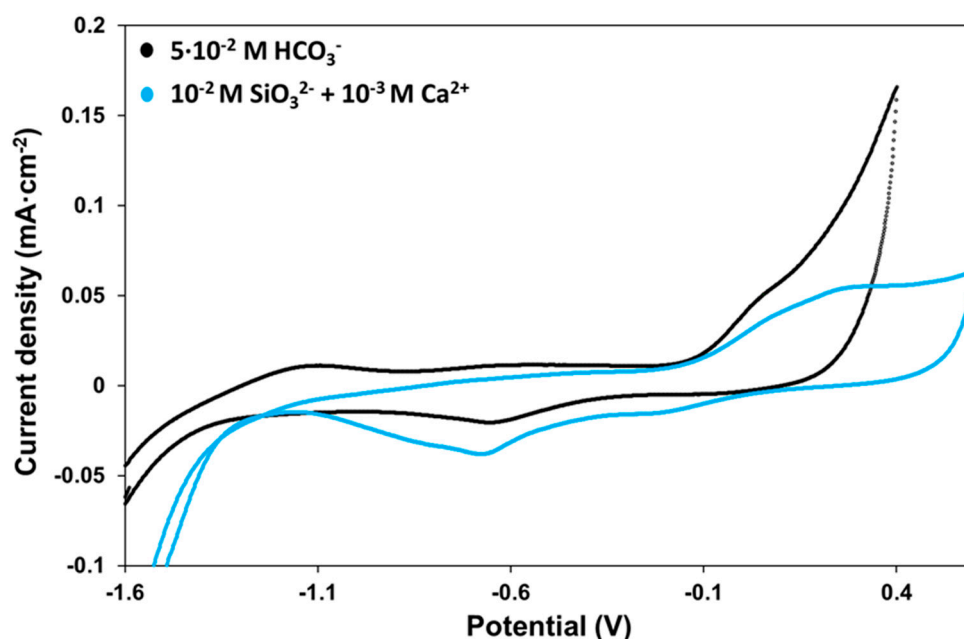


Figure 4. CVs recorded at a scan rate of $10 \text{ mV}\cdot\text{s}^{-1}$ (rotation rate of 1000 rpm) on 5 wt.% Gd_2O_3 -doped UO_2 electrode in a solution that contains 0.1 M NaCl, $10^{-2} \text{ M SiO}_3^{2-}$ and $10^{-3} \text{ M Ca}^{2+}$ (blue) and in a solution that contains 0.1 M NaCl and $5 \times 10^{-2} \text{ M HCO}_3^-$ (black). The potential was scanned from -1.6 V to 0.6 V and back. Both dissolutions were adjusted at pH 10.

The suppression of the anodic dissolution could be probably attributed to the adsorption of silicate and calcium to the electrode surface. These results are in good agreement with the findings of Wilson and Gray [4], as they detected in leaching experiments a thin layer of Ca and Si, which inhibited the dissolution of UO_2 . Further investigation in solutions containing Ca, Si and carbonates, which better mimic cementitious water, may be needed to determine whether the predominant factor is the formation of soluble ternary complexes Ca-U(VI)-CO_3 [24] or the inhibitory effects of Ca and Si.

2.3. Potentiostatic Oxidation

Since CVs are rapid experiments, to better observe differences in reactivity due to doping level, potentiostatic oxidation experiments were performed. Figure 5 shows a series of current density vs. time plots recorded at an oxidative potential of 0.4 V for 1 h for the different electrodes in a solution with silicate and calcium. In general, for all electrodes, the anodic current decreases linearly on the logarithm scale with time, which is consistent with a loss of surface reactivity due to the growth of a $\text{U}^{\text{IV/V}}\text{O}_{2+x}$ surface layer [19].

For the non-doped electrode, the current density registered was considerably higher than in doped electrodes. After 1000 s the current tends toward a steady-state value (reaches a plateau). Regarding doped electrodes, 5 wt.% Gd_2O_3 -doped UO_2 electrode registered at short times higher current densities compared to 10 wt.% Gd_2O_3 -doped UO_2 electrode, while at long times, the currents continued decreasing, reaching very low values for both electrodes.

Figure 6 shows the cumulative integration of the potentiostatic current densities (from Figure 5) as a function of time for the three electrodes. The general trend observed is that the charge accumulated increases as the doping level decreases. Whereas the total charge for the non-doped electrode continues increasing with time in the period of time registered (3600 s), for doped electrodes their respective total charges tend to reach a stable state.

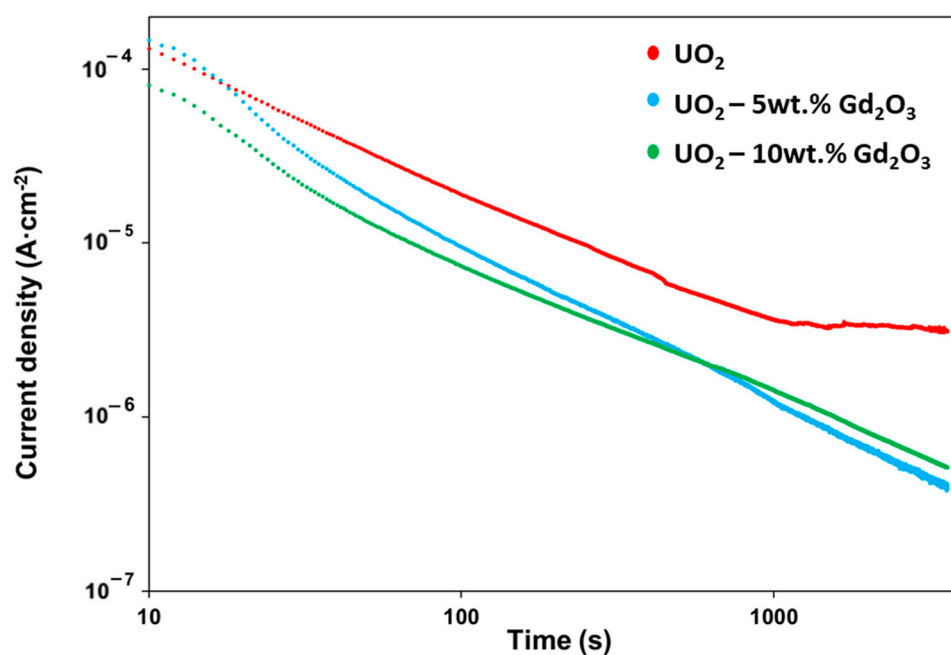


Figure 5. Potentiostatic current-time curves recorded at 0.4 V for 1 h on the three different electrodes in a solution that contains 0.1 M NaCl, 10^{-2} M SiO_3^{2-} and 10^{-3} M Ca^{2+} .

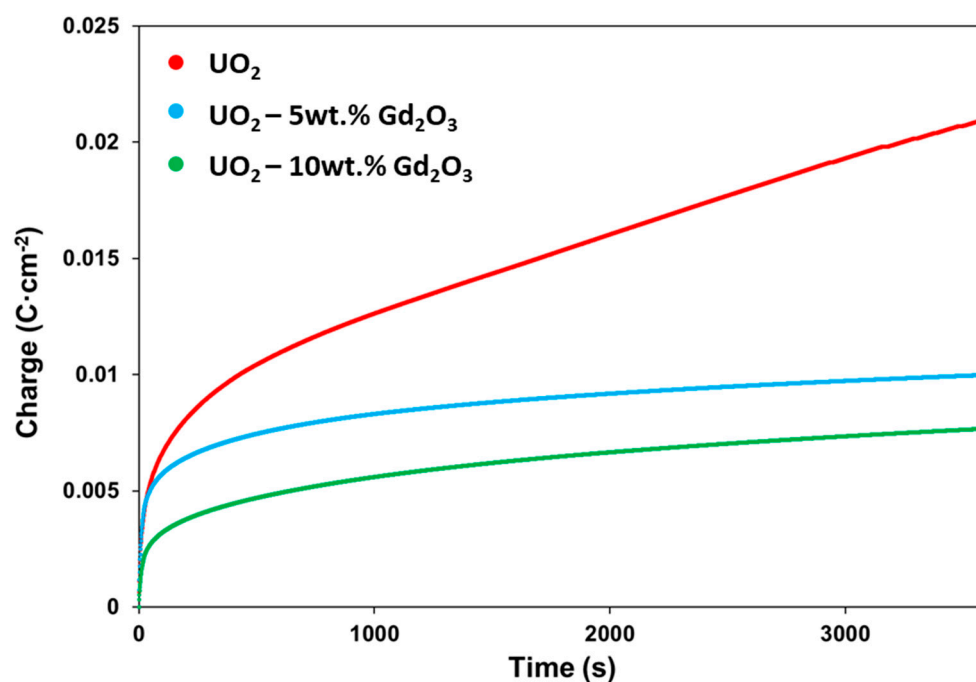


Figure 6. Cumulative anodic charges obtained by integration of the current densities registered from potentiostatic experiments in a solution that contains 0.1 M NaCl, 10^{-2} M SiO_3^{2-} and 10^{-3} M Ca^{2+} at 0.4 V for 1 h on the three electrodes as a function of time.

XPS was performed after potentiostatic experiments to determine the composition of the electrode surface as a function of the extent of doping. Figure 7 shows the deconvoluted spectra for the U $4f_{5/2}$ and U $4f_{7/2}$ regions and their corresponding satellite structures for the three different electrodes while Table 1 collects the percentages of U^{IV} , U^{V} and U^{VI} on the electrodes surface. In all cases, as expected, traces of U^{IV} were detected, whereas U^{V} and U^{VI} states dominate the surface composition of the electrodes, since an oxidizing potential was applied. This is consistent with the formation of an underlying $\text{U}^{\text{IV}}_{1-2x}\text{U}^{\text{V}}_{2x}\text{O}_{2+x}$

layer and the following formation of UO_2^{2+} , which can be accumulated as a $\text{U}^{\text{VI}}\text{O}_3 \cdot y\text{H}_2\text{O}$ deposit. It can be observed that as the doping level increases, the U^{V} content increases, at the expense of U^{VI} . Although the effect of doping with 5 wt.% Gd_2O_3 is small, in the 10 wt.% Gd_2O_3 - UO_2 electrode, a strong U^{V} signal was obtained, which is consistent with a marked decrease in reactivity at high doping levels (10%), as already reported in the literature [7]. The differences observed in U^{VI} concentration provide evidence that doping with Gd_2O_3 slows down the second oxidation step ($\text{U}^{\text{IV}}_{1-2x}\text{U}^{\text{V}}_{2x}\text{O}_{2+x}$ to $\text{U}^{\text{VI}}\text{O}_3 \cdot y\text{H}_2\text{O}$). These results are in agreement with the potentiostatic data, since lower anodic charges lead to lower amount of U^{VI} and hence, lower oxidation.

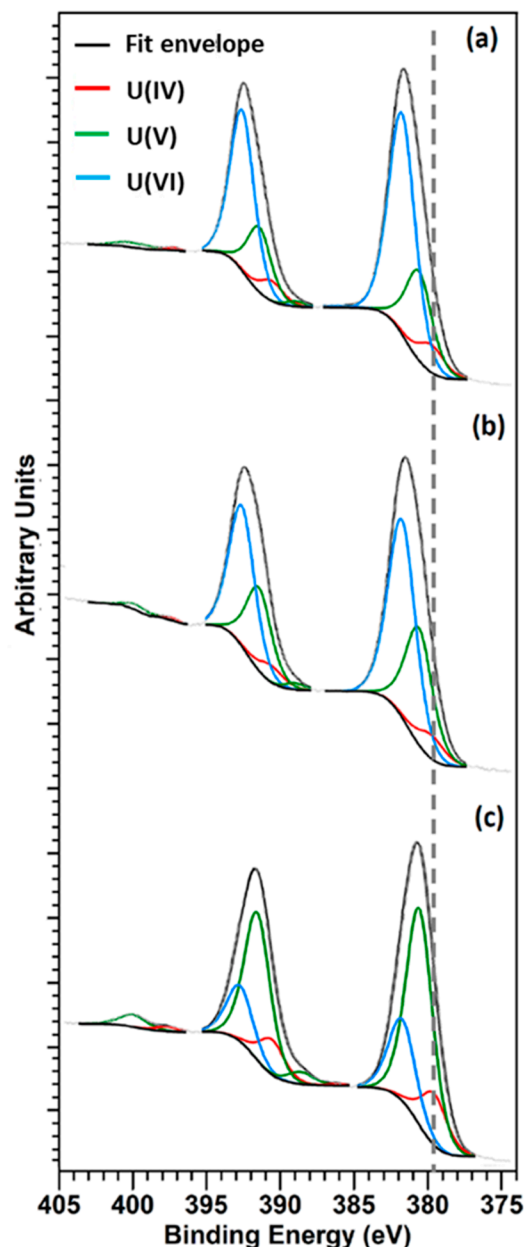


Figure 7. U 4f XPS spectra resolved into U^{IV} , U^{V} and U^{VI} contributions recorded after potentiostatic oxidation at 0.4 V on (a) undoped UO_2 electrode, (b) 5 wt.% Gd_2O_3 -doped UO_2 electrode and (c) 10 wt.% Gd_2O_3 -doped UO_2 electrode. The vertical dashed line represents the position of U^{IV} at 379.7 eV.

Table 1. Relative fractions of U^{IV}, U^V and U^{VI} on the surface of the different samples from XPS results after potentiostatic oxidation at 0.4 V.

Sample	U ^{IV} (%)	U ^V (%)	U ^{VI} (%)
UO ₂	8 ± 5	26 ± 5	66 ± 5
UO ₂ —5 wt.% Gd ₂ O ₃	7 ± 5	35 ± 5	58 ± 5
UO ₂ —10 wt.% Gd ₂ O ₃	15 ± 5	62 ± 5	23 ± 5

This observation is consistent with the results reported in air oxidation by Scheele et al. [25], who observed a delay on the onset of the second oxidation to U₃O₈ on Gd₂O₃-UO₂ doped samples. XPS analysis performed after dissolution experiments in presence of carbonate/bicarbonate [12] revealed a big contribution of U(V) on the surface of the Gd₂O₃-UO₂ samples, and low U concentration on the leaching, indicating that Gd-doping enhanced the stability of U(V) and inhibited the subsequent oxidation to U(VI). A decrease in the uranium concentration on Gd-doped UO₂ pellets was also reported in leaching experiments in H₂O₂ and γ -irradiation [13]. Similar behaviour was found in the literature for Nd-doped UO₂ in presence of H₂O₂ [26]. This found could indicate that doping UO₂ with trivalent dopants (like Gd³⁺ and Nd³⁺) would lead to a comparable stabilization effect on the UO₂ structure.

2.4. Cathodic Stripping Voltammetry

Additional potentiostatic experiments were performed at the same conditions (0.4 V for 1 h), but this time followed by cathodic stripping voltammetry (CSV) in order to reduce the surface layer and the deposit. Figure 8 shows the CSV recorded for the three electrodes. Two reduction peaks were observed in this region, which are commonly assigned to the reduction of the dual phase nature of U^{IV}_{1-2x}U^V_{2x}O_{2+x}/U^{VI}O₃·yH₂O. The reduction peak observed at -0.7 V (peak 1 in Figure 8) was attributed previously to the reduction of the underlying U^{IV}_{1-2x}U^V_{2x}O_{2+x} layer [21,22], whereas the second peak located at -0.8 V (peak 2 in Figure 8) was assigned to the reduction of UO₃·yH₂O deposit [15].

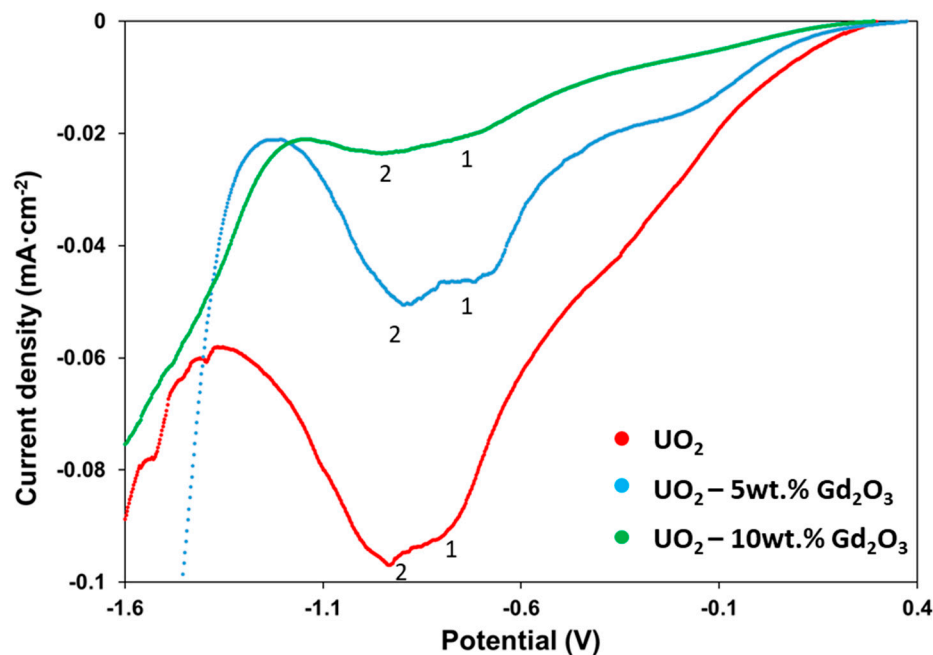


Figure 8. Cathodic stripping voltammograms (CSV) recorded on the different electrodes after potentiostatic oxidation in a solution that contains 0.1 M NaCl, 10⁻² M SiO₃²⁻ and 10⁻³ M Ca²⁺. The potential was scanned from 0.4 V to -1.6 V at a scan rate of 10 mV·s⁻¹.

The current peaks can be considered as a measure of the thickness of the oxidized surface layer. Hence, the thickness of the $U^{IV}_{1-2x}U^{V}_{2x}O_{2+x}/U^{VI}O_3 \cdot yH_2O$ layer was lower as the Gd_2O_3 doping level increases. These results are in agreement with the current densities registered in the potentiostatic oxidation experiments (Figure 5).

2.5. Corrosion Potential

Figure 9 shows the corrosion potential (E_{CORR}) registered on each electrode. The horizontal line at -0.4 V represents the threshold for the onset of fuel corrosion. For all electrodes, the values of E_{CORR} increased quickly from the cathodic cleaning potential (-1.6 V) until achieving a steady state value. The values of E_{CORR} recorded after 24 h were -0.10 V, -0.14 V and -0.27 V for undoped UO_2 electrode, 5 wt.% Gd_2O_3 and 10 wt.% Gd_2O_3 doped UO_2 electrodes, respectively, which are substantially more negative as the doping level increases, indicating an influence of the electrode composition on the E_{CORR} .

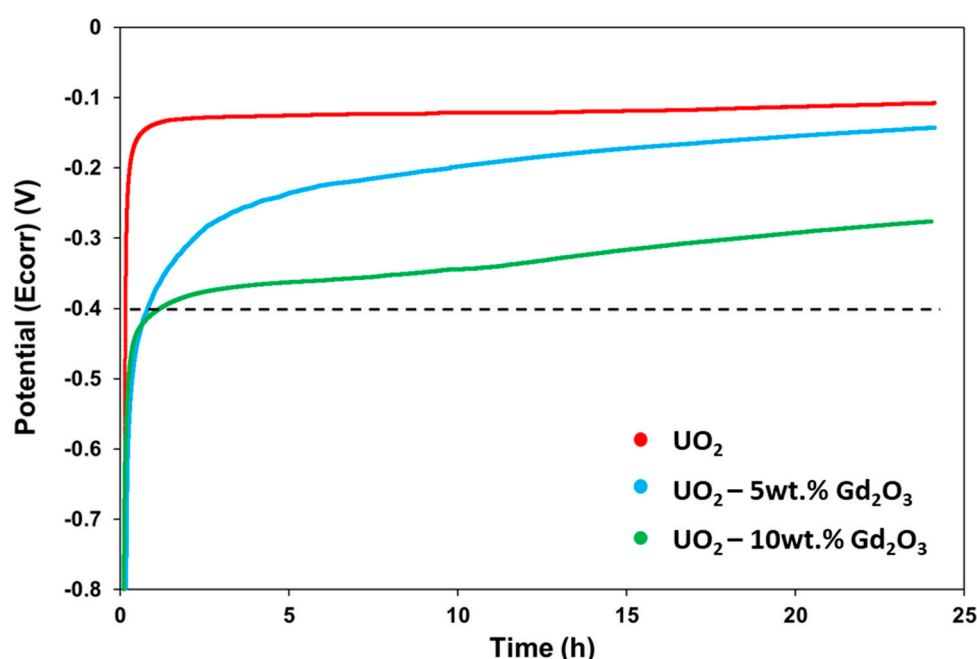


Figure 9. E_{CORR} measurements recorded on the three different electrodes in a solution that contains 0.1 M NaCl, 10^{-2} M SiO_3^{2-} and 10^{-3} M Ca^{2+} . The horizontal dashed line at -0.4 V indicates the threshold potential for the beginning of oxidation of the UO_2 .

Figure 10 shows the XPS analysis performed after E_{CORR} measurements and Table 2 displays the fraction of the individual oxidation states of uranium (expressed as percentages) on the electrode surfaces. U^{IV} is the dominant oxidation state present in the 10 wt.% Gd_2O_3 doped UO_2 electrode surface (around 87%), whereas both undoped and 5 wt.% Gd_2O_3 doped electrodes surfaces are predominantly composed of the oxidation states U^{IV} and U^V , being the U^{IV} content slightly higher in the doped electrode than in the undoped one. A low amount of U^{VI} was detected in UO_2 electrode (14%) while in doped electrodes the amount was almost negligible (below 4%). As mentioned before, silicate and calcium could be adsorbed on the electrode surface, which could partially inhibit the further oxidation of the thin surface layer [19] at such conditions.

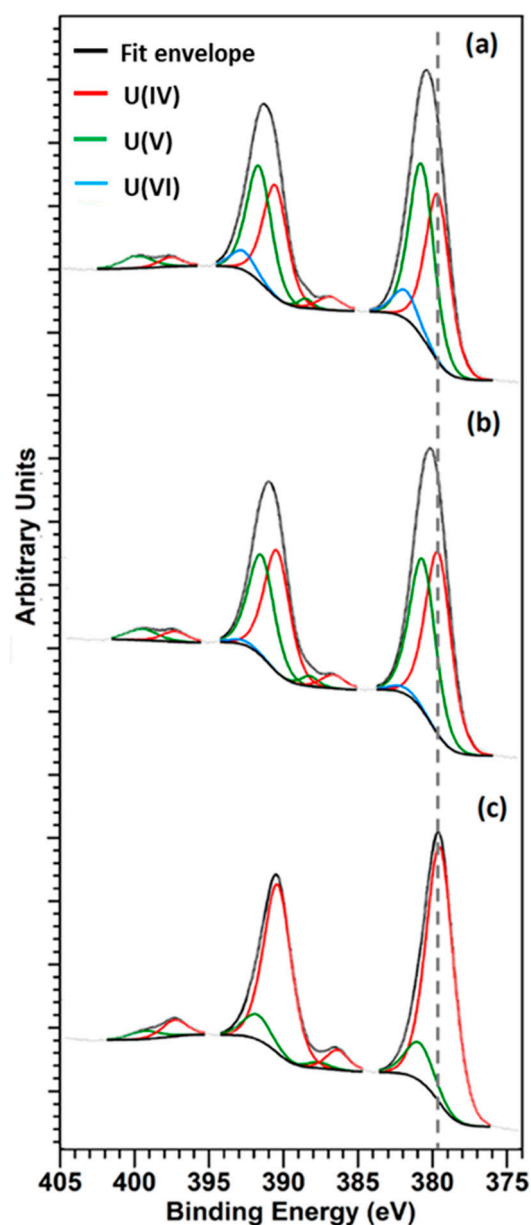


Figure 10. U 4f XPS spectra resolved into U^{IV} , U^V and U^{VI} contributions recorded after E_{CORR} experiments on (a) undoped UO_2 electrode, (b) 5 wt.% Gd_2O_3 -doped UO_2 electrode and (c) 10 wt.% Gd_2O_3 -doped UO_2 electrode. The vertical dashed line represents the position of U^{IV} at 379.7 eV.

Table 2. Relative fractions of U^{IV} , U^V and U^{VI} on the surface of the different samples from XPS results after corrosion potential experiments.

Sample	U^{IV} (%)	U^V (%)	U^{VI} (%)
UO_2	38 ± 5	48 ± 5	14 ± 5
UO_2 —5 wt.% Gd_2O_3	49 ± 5	47 ± 5	4 ± 5
UO_2 —10 wt.% Gd_2O_3	87 ± 5	13 ± 5	0 ± 5

Shoesmith et al. reported a reaction sequence on unirradiated UO_2 electrodes in basic solutions in terms of E_{CORR} [27]. For $E_{CORR} < -0.1$ V, the oxidation of UO_2 surface occurs, as a thin surface layer U^{IV}/U^V is being formed. Therefore, it is expected that the oxidized states U^{IV} and U^V dominates the surface composition. The surface becomes more oxidized as E_{CORR} increases. For $E_{CORR} \geq -0.1$ V, the oxidative dissolution of the oxidized layer (as UO_2^{2+}) occurs, hence the presence of U^{VI} is expected as no complexing agents like

bicarbonate are present in the solution. For $E_{\text{CORR}} > 0$ V, the formation of secondary phases (in the form of $\text{UO}_3 \cdot \text{H}_2\text{O}$) is expected to take place on the electrode surface.

According to our XPS measurements, the composition of the surface obtained after the corrosion experiments are consistent with E_{CORR} values registered at steady state. For undoped UO_2 electrode, the presence of U^{VI} can be explained due to oxidative dissolution explained for $E_{\text{CORR}} \geq -0.1$ V. For doped electrodes, only the oxidation of UO_2 surface occurs, as no U^{VI} was significantly measured ($E_{\text{CORR}} < -0.1$ V). However, in the 10 wt.% Gd_2O_3 electrodes, only a slight oxidation of the UO_2 surface (U^{V} composition of 13%) was observed, which is in agreement with the low E_{CORR} value obtained (-0.27 V, close to the oxidation threshold). On the contrary, the 5 wt.% Gd_2O_3 doped UO_2 electrode registered a higher E_{CORR} (-0.14 V) and a higher degree of oxidation (U^{V} composition of 47%).

These results would confirm that the formation of the thin surface layer $\text{U}^{\text{IV}}/\text{U}^{\text{V}}$ was influenced by Gd^{III} -doping in the presence of silicate and calcium. Such retardation of the oxidation process can be attributed to the ability of Gd to delay the incorporation of O^{2-} into interstitial sites within the fluorite lattice of the UO_2 surface [7,15]. This effect was particularly marked at high doping levels (10 wt.% Gd_2O_3). However, despite the similar E_{CORR} values achieved for undoped UO_2 and UO_2 doped with 5 wt.% Gd_2O_3 , a more rapid oxidation on the undoped UO_2 electrode was observed (the rate of rise of E_{CORR} was higher for the undoped electrode), evidencing a clear decrease in reactivity due to Gd_2O_3 .

3. Materials and Methods

3.1. Electrode Preparation

Undoped UO_2 and UO_2 doped with 5 wt.% and 10 wt.% Gd_2O_3 pellets were fabricated by mixing fine-grained powders of UO_2 (supplied by ENUSA, Madrid, Spain) and Gd_2O_3 powders (99.9%, supplied by Sigma Aldrich, St. Louis, MO, USA). The powders were compacted into pellets by means of a hydraulic press and sintered in a horizontal tube furnace (ST196030 HG from Hobersal, Barcelona, Spain) at 1740 °C for 9 h in a reducing atmosphere (5% hydrogen in 95% argon), based on the methodology explained by Baena et al. [28]. This methodology was confirmed to be adequate for obtaining successfully sintered Gd_2O_3 -doped UO_2 pellets [12]. The pellets, with a thickness of 3 mm and a diameter of 12 mm, were characterised by scanning electron microscopy (SEM) and X-ray diffraction (XRD). Then, to study the electrochemical behaviour of the pellets, electrodes were prepared from the pellets by following the procedure described in the literature [29]. First, in order to improve the electrical conductivity, one face of the pellet was electroplated with copper. For that purpose, the pellet was fitted at the end of a rubber tube, with the face to be plated exposed to a solution of $0.1 \text{ mol} \cdot \text{L}^{-1}$ CuSO_4 and a Cu metal wire immersed as a cathode. Mercury (Thermo Scientific, Waltham, MA, USA) was poured into the rubber tube to make an electrical contact between the pellet and a stainless-steel wire, acting as an anode. A 10 mA current was applied for 5 min by using a laboratory power supply Manson EP-613 (Kwai Chung, Hong Kong). The Cu-plated side of the pellet was connected to a stainless-steel threaded post by using a conductive silver epoxy (8331-14G). The pellet was embedded with a non-conductive epoxy EE 9466 resin so that only one side of the electrode is in contact with the solution. The electrode was left to cure overnight in a vacuum desiccator. The threaded stainless-steel post was screwed onto the shaft of a rotating disk electrode (Metrohm, Herisau, Switzerland). Both the electrode and stainless-steel shaft were tightly wrapped with poly(tetrafluoroethylene) (PTFE) to avoid entering in contact with the solution. Prior to any experiment, the electrode was abraded using wet SiC paper (1200 grit) and rinsed with distilled deionized water to remove any oxidized surface phase.

3.2. Electrochemical Cell and Equipment

Electrochemical experiments were conducted in a single compartment corrosion cell Autolab 1 L model from Metrohm (Herisau, Switzerland). A standard three-electrode set-up was used with some electrodes of UO_2 (doped with 0, 5 and 10 wt.% Gd_2O_3) as working electrode, the counter electrode was a platinum sheet (surface area $\sim 1 \text{ cm}^2$) and the

reference electrode was an Ag/AgCl (3 M KCl) electrode. All potential values are recorded versus the Ag/AgCl standard reference electrode (+0.208 V, 25 °C vs. standard hydrogen electrode (SHE)). Experiments were conducted at room temperature. All electrochemical experiments were performed using Multi Autolab Potentiostat-Galvanostat M204 from Metrohm, (Herisau, Switzerland). NOVA software 2.1 (Metrohm, Herisau, Switzerland) was used to record and to analyse the data.

3.3. Electrochemical Techniques

Four general types of electrochemical techniques were carried out: cyclic voltammetry (CV), potentiostatic oxidation, cathodic stripping voltammetry (CSV) and corrosion potential (E_{CORR}). Prior to any experiment, the electrode was cathodically cleaned for 120 s at -1.6 V to remove U^{VI} oxides present on the surface. CV is a potential tool to investigate the potential at which UO_2 undergoes oxidation or reduction in a solution. In that regard, the potential (V) was scanned from -1.6 V to 0.6 V and back at a rate of $10 \text{ mV}\cdot\text{s}^{-1}$ while recording the current. The electrode rotation rate was held constant at 1000 rpm. In potentiostatic oxidation experiments, a constant anodic potential of 0.4 V was applied to the electrode for an hour and current-time profiles were recorded. This technique is capable of identifying variations in oxidation rates and levels of the electrode at a specific oxidizing potential due to Gd doping. After the anodic oxidation, the surface of the electrode was analysed by XPS. Immediately after a second set of identical potentiostatic oxidation experiments, cathodic stripping voltammetry was conducted in order to reduce the oxidized surface layer formed on the electrode. The cathodic charge measured can serve as an indicator of the layer thickness. This was performed by scanning the potential from the potentiostatic oxidation potential (0.4 V) to -1.6 V at a scan rate of $10 \text{ mV}\cdot\text{s}^{-1}$, while the current was registered. Finally, in the corrosion potential experiments, the working electrode was immersed in the solution for 24 h, while the potential that exists across the electrodes and electrolyte was measured in the absence of any current flow. This measurement serves as an indicator of the tendency of an electrode to corrode in a specific environment and XPS analysis was performed after the E_{CORR} measurement.

3.4. Solution

The solution used for all experiments was $0.1 \text{ mol}\cdot\text{dm}^{-3}$ NaCl (99.0%, Sigma Aldrich, St. Louis, MO, USA) as a supporting electrolyte, containing $10^{-2} \text{ mol}\cdot\text{dm}^{-3}$ SiO_3^{2-} ($\text{Na}_2\text{SiO}_3\cdot 5\text{H}_2\text{O}$ (99.0%, Sigma Aldrich, St. Louis, MO, USA)) and $10^{-3} \text{ mol}\cdot\text{dm}^{-3}$ Ca^{2+} (CaCl_2 (99.0%, Sigma Aldrich, St. Louis, MO, USA)). In addition, for testing the performance of the electrodes in cyclic voltammetry experiments, a solution that contained $0.1 \text{ mol}\cdot\text{dm}^{-3}$ NaCl (99.0%, Sigma Aldrich, St. Louis, MO, USA) and $5\cdot 10^{-2} \text{ mol}\cdot\text{dm}^{-3}$ of NaHCO_3 (99.0%, Sigma Aldrich, St. Louis, MO, USA) was prepared. All solutions were prepared using ultrapure water obtained from a Milli-Q water purification system (Merck, Darmstadt, Germany). The pH of the solutions was adjusted to 10 using HCl or NaOH and measured with an Orion model 720A pH meter (Waltham, MA, USA). The pH was measured periodically and did not vary more than 1% throughout the experiments. The solutions were bubbled with N_2 (99.99%, Nippon Gases, Tokyo, Japan) before any experiment for 1 h to purge and during the experiments.

3.5. XPS Analysis

XPS analyses were performed to observe changes in the oxidation of the electrode surface after potentiostatic oxidation and corrosion potential experiments. A SPECS system equipment (Berlin, Germany) with an Al anode XR50 source operating at 150 W and a Phoibos MCD-9 detector was used. The sensitivity of the equipment was ± 0.1 eV of binding energy (BE). The spectra were recorded at a pressure below 10^{-8} mbar. The spectra were evaluated using CasaXPS software (Casa Software Ltd., Teignmouth, UK) version 2.3.25. C 1s peak was set at 285.0 eV to correct surface charging. The spectra were fitted using a 30% of Lorentzian curve and 70% of Gaussian curve with a Shirley background

correction. The $U4f_{7/2}$ and $U4f_{5/2}$ regions were used to determine the total amount of each uranium oxidation state (U^{IV} , U^V and U^{VI}) by the deconvolution of the peaks [30–34]. The position of the satellite peaks was used to validate the curve-fitting procedure.

Before transferring to the XPS spectrometer for XPS measurements, electrodes were removed from the electrochemical cell, gently rinsed with MilliQ water to remove electrolyte residue and dried in a desiccator.

3.6. SEM Measurements

A Phenom XL scanning electron microscope coupled to an energy dispersive X-ray detector (EDX) from PhenomWorld (Waltham, MA, USA) was used to analyse the microstructure of the samples.

3.7. X-ray Diffraction (XRD)

A Bruker D8 diffractometer (Karlsruhe, Germany) with an X-ray source of Cu $K\alpha$ radiation ($\lambda = 1.54056 \text{ \AA}$) at 45 kV and 35 mA was used to analyse the crystal structure of the samples.

4. Conclusions

The effect of Gd (5 wt.% and 10 wt.% Gd_2O_3) on the electrochemical behaviour of UO_2 was investigated in a slightly alkaline solution in the presence of silicate and calcium. Cyclic voltammetry experiments showed that the anodic oxidation/dissolution mechanism on Gd_2O_3 - UO_2 was similar to that on undoped UO_2 electrode. However, the corrosion process of doped UO_2 decreases, as lower current densities were registered. Both potentiostatic and E_{CORR} experiments showed that such retardation effect was small when doping with 5 wt.% Gd_2O_3 , however, it was strongly enhanced when Gd_2O_3 content is around 10 wt.% Gd_2O_3 . This behaviour is commonly attributed to the reduction in the availability of oxygen vacancies to accommodate O^{2-} ions during oxidation in the UO_2 lattice, as Gd^{III} -O vacancy clusters might be formed.

In addition, the presence of silicate and calcium in solution was found to have influence on the oxidation of UO_2 , leading to a suppression of anodic dissolution probably due to the adsorption of these ions on the electrode surface. This is in contrast to solutions that contain bicarbonate ions, which are known to form soluble complexes with UO_2^{2+} and to accelerate UO_2 corrosion. Additional experiments with solution containing Ca, Si and carbonate would be required to investigate which effect would predominate.

In conclusion, both Gd_2O_3 doping and the presence of silicate and calcium in solution are factors that decrease the reactivity of UO_2 , which is beneficial for the assessment of repository safety, as an important fraction of the radionuclide release would be inhibited.

Author Contributions: Conceptualization, I.C. and J.D.P.; methodology, I.C.; writing—original draft, S.G.-G.; writing—review and editing, I.C., J.D.P., J.G. and J.L.; validation, S.G.-G.; funding acquisition, J.D.P. All authors have read and agreed to the published version of the manuscript.

Funding: This research was funded by Ministerio de Economía y Competitividad (Spain) with the projects ENE2017-83048-R and PID2020-116839RB-I00. ENRESA is also acknowledged for its interest and financial support (Project 079-CO-IA-2020-0001 and CO-IA-22-010). S. García-Gómez wants to acknowledge the fellowship with reference code PRE2018-085618. Financial support was also received from the Catalan AGAUR Agency through the Research Groups Support program (grant number: 2021-SGR-GRC-00596).

Data Availability Statement: Data is available on request.

Acknowledgments: J. Llorca is a Serra Húnter Fellow and is grateful to the ICREA Academia program.

Conflicts of Interest: The authors declare no conflict of interest.

References

1. He, H.; Keech, P.G.; Broczkowski, M.E.; Noël, J.J.; Shoesmith, D.W. Characterization of the Influence of Fission Product Doping on the Anodic Reactivity of Uranium Dioxide. *Can. J. Chem.* **2007**, *85*, 702–713. [[CrossRef](#)]
2. Razdan, M.; Shoesmith, D.W. Influence of Trivalent-Dopants on the Structural and Electrochemical Properties of Uranium Dioxide (UO₂). *J. Electrochem. Soc.* **2014**, *161*, H105–H113. [[CrossRef](#)]
3. Kim, J.G.; Ha, Y.K.; Park, S.D.; Jee, K.Y.; Kim, W.H. Effect of a Trivalent Dopant, Gd³⁺, on the Oxidation of Uranium Dioxide. *J. Nucl. Mater.* **2001**, *297*, 327–331. [[CrossRef](#)]
4. Wilson, C.N.; Gray, W.J. Measurement of Soluble Nuclide Dissolution Rates from Spent Fuel. *MRS Proc.* **1989**, *176*, 489–498. [[CrossRef](#)]
5. Leinweber, G.; Barry, D.P.; Trbovich, M.J.; Burke, J.A.; Drindak, N.J.; Knox, H.D.; Ballard, R.V.; Block, R.C.; Danon, Y.; Severnyak, L.I. Neutron Capture and Total Cross-Section Measurements and Resonance Parameters of Gadolinium. *Nucl. Sci. Eng.* **2006**, *154*, 261–279. [[CrossRef](#)]
6. Lee, J.; Kim, J.Y.G.J.; Youn, Y.S.; Liu, N.; Kim, J.Y.G.J.; Ha, Y.K.; Shoesmith, D.W.; Kim, J.Y.G.J. Raman Study on Structure of U_{1-y}Gd_yO_{2-x} (Y = 0.005, 0.01, 0.03, 0.05 and 0.1) Solid Solutions. *J. Nucl. Mater.* **2017**, *486*, 216–221. [[CrossRef](#)]
7. Liu, N.; Kim, J.; Lee, J.; Youn, Y.S.; Kim, J.G.; Kim, J.Y.; Noël, J.J.; Shoesmith, D.W. Influence of Gd Doping on the Structure and Electrochemical Behavior of UO₂. *Electrochim. Acta* **2017**, *247*, 496–504. [[CrossRef](#)]
8. Scheele, R.D.; Hanson, B.D.; Casella, A.M. Effect of Added Gadolinium Oxide on the Thermal Air Oxidation of Uranium Dioxide. *J. Nucl. Mater.* **2021**, *552*, 153008. [[CrossRef](#)]
9. García-Gómez, S.; Giménez, J.; Casas, I.; Llorca, J.; De Pablo, J. X-ray Photoelectron Spectroscopy (XPS) Study of Surface Oxidation of UO₂ Doped with Gd₂O₃ at Different Temperatures and Atmospheres. *Appl. Surf. Sci.* **2023**, *629*, 157429. [[CrossRef](#)]
10. Kim, J.; Lee, J.; Youn, Y.S.; Liu, N.; Kim, J.G.; Ha, Y.K.; Bae, S.E.; Shoesmith, D.W.; Kim, J.Y. The Combined Influence of Gadolinium Doping and Non-Stoichiometry on the Structural and Electrochemical Properties of Uranium Dioxide. *Electrochim. Acta* **2017**, *247*, 942–948. [[CrossRef](#)]
11. Casella, A.; Hanson, B.; Miller, W. The Effect of Fuel Chemistry on UO₂ Dissolution. *J. Nucl. Mater.* **2016**, *476*, 45–55. [[CrossRef](#)]
12. García-Gómez, S.; Giménez, J.; Casas, I.; Llorca, J.; De Pablo, J. Oxidative Dissolution Mechanism of Both Undoped and Gd₂O₃-Doped UO₂(s) at Alkaline to Hyperalkaline pH. *Dalton Trans.* **2023**, *52*, 9823–9830. [[CrossRef](#)] [[PubMed](#)]
13. Barreiro Fidalgo, A.; Jonsson, M. Radiation Induced Dissolution of (U, Gd)O₂ Pellets in Aqueous Solution—A Comparison to Standard UO₂ Pellets. *J. Nucl. Mater.* **2019**, *514*, 216–223. [[CrossRef](#)]
14. Park, K.; Olander, D.R. Defect Models for the Oxygen Potentials of Gadolinium-and Europium-Doped Urania. *J. Nucl. Mater.* **1992**, *187*, 89–96. [[CrossRef](#)]
15. Razdan, M.; Shoesmith, D.W. The Electrochemical Reactivity of 6.0 Wt% Gd-Doped UO₂ in Aqueous Carbonate/Bicarbonate Solutions. *J. Electrochem. Soc.* **2014**, *161*, H225–H234. [[CrossRef](#)]
16. Heath, T.; Schofield, J.; Shelton, A. Understanding Cementitious Backfill Interactions with Groundwater Components. *Appl. Geochem.* **2020**, *113*, 104495. [[CrossRef](#)]
17. Huertas, F.J.; Hidalgo, A.; Rozalén, M.L.; Pellicione, S.; Domingo, C.; García-González, C.A.; Andrade, C.; Alonso, C. Interaction of Bentonite with Supercritically Carbonated Concrete. *Appl. Clay Sci.* **2009**, *42*, 488–496. [[CrossRef](#)]
18. Santos, B.G.; Noël, J.J.; Shoesmith, D.W. The Influence of Calcium Ions on the Development of Acidity in Corrosion Product Deposits on SIMFUEL, UO₂. *J. Nucl. Mater.* **2006**, *350*, 320–331. [[CrossRef](#)]
19. Santos, B.G.; Noël, J.J.; Shoesmith, D.W. The Influence of Silicate on the Development of Acidity in Corrosion Product Deposits on SIMFUEL (UO₂). *Corros. Sci.* **2006**, *48*, 3852–3868. [[CrossRef](#)]
20. Espriu-Gascon, A.; Shoesmith, D.W.; Giménez, J.; Casas, I.; de Pablo, J. Study of SIMFUEL Corrosion under Hyper-Alkaline Conditions in the Presence of Silicate and Calcium. *MRS Adv.* **2017**, *2*, 543–548. [[CrossRef](#)]
21. Shoesmith, D.W. Used Fuel and Uranium Dioxide Dissolution Studies—A Review. In Proceedings of the Corrosion Conference and Expo (Corrosion 2008), New Orleans, LA, USA, 16–20 March 2008; p. 56.
22. Shoesmith, D.W. Fuel Corrosion Processes under Waste Disposal Conditions. *J. Nucl. Mater.* **2000**, *282*, 1–31. [[CrossRef](#)]
23. Keech, P.G.; Goldik, J.S.; Qin, Z.; Shoesmith, D.W. The Anodic Dissolution of SIMFUEL (UO₂) in Slightly Alkaline Sodium Carbonate/Bicarbonate Solutions. *Electrochim. Acta* **2011**, *56*, 7923–7930. [[CrossRef](#)]
24. Maia, F.M.S.; Ribet, S.; Bailly, C.; Grivé, M.; Madé, B.; Montavon, G. Evaluation of Thermodynamic Data for Aqueous Ca-U(VI)-CO₃ Species under Conditions Characteristic of Geological Clay Formation. *Appl. Geochem.* **2021**, *124*, 104844. [[CrossRef](#)]
25. Scheele, R.D.; Hanson, B.D.; Cumblidge, S.E.; Jenson, E.D.; Kozelisky, A.E.; Sell, R.L.; Macfarlan, P.J.; Snow, L.A. Effect of Gadolinium Doping on the Air Oxidation of Uranium Dioxide. *Mat. Res. Soc. Symp. Proc.* **2004**, *824*, CC8.8.1–CC8.8.6. [[CrossRef](#)]
26. Kegler, P.; Neumeier, S.; Klinkenberg, M.; Bukaemskiy, A.; Deissmann, G.; Brandt, F.; Bosbach, D. Accelerated Dissolution of Doped UO₂-Based Model Systems as Analogues for Modern Spent Nuclear Fuel under Repository Conditions. *MRS Adv.* **2023**, *8*, 255–260. [[CrossRef](#)]
27. Shoesmith, D.W.; Sunder, S.; Bailey, M.G.; Miller, N.H. Corrosion of Used Nuclear Fuel in Aqueous Perchlorate and Carbonate Solutions. *J. Nucl. Mater.* **1996**, *227*, 287–299. [[CrossRef](#)]
28. Baena, A.; Cardinaels, T.; Vos, B.; Binnemans, K.; Verwerft, M. Synthesis of UO₂ and ThO₂ Doped with Gd₂O₃. *J. Nucl. Mater.* **2015**, *461*, 271–281. [[CrossRef](#)]

29. Ofori, D.; Keech, P.G.; Noël, J.J.; Shoesmith, D.W. The Influence of Deposited Films on the Anodic Dissolution of Uranium Dioxide. *J. Nucl. Mater.* **2010**, *400*, 84–93. [[CrossRef](#)]
30. Ilton, E.S.; Bagus, P.S. XPS Determination of Uranium Oxidation States. *Surf. Interface Anal.* **2011**, *43*, 1549–1560. [[CrossRef](#)]
31. Ilton, E.S.; Boily, J.F.; Bagus, P.S. Beam Induced Reduction of U(VI) during X-Ray Photoelectron Spectroscopy: The Utility of the U4f Satellite Structure for Identifying Uranium Oxidation States in Mixed Valence Uranium Oxides. *Surf. Sci.* **2007**, *601*, 908–916. [[CrossRef](#)]
32. Teterin, Y.A.; Popel, A.J.; Maslakov, K.I.; Teterin, A.Y.; Ivanov, K.E.; Kalmykov, S.N.; Springell, R.; Scott, T.B.; Farnan, I. XPS Study of Ion Irradiated and Unirradiated UO₂ Thin Films. *Inorg. Chem.* **2016**, *55*, 8059–8070. [[CrossRef](#)] [[PubMed](#)]
33. Schindler, M.; Hawthorne, F.C.; Freund, M.S.; Burns, P.C. XPS Spectra of Uranyl Minerals and Synthetic Uranyl Compounds. I: The U 4f Spectrum. *Geochim. Cosmochim. Acta* **2009**, *73*, 2471–2487. [[CrossRef](#)]
34. Boily, J.F.; Ilton, E.S. An Independent Confirmation of the Correlation of U4f Primary Peaks and Satellite Structures of U^{VI}, U^V and U^{IV} in Mixed Valence Uranium Oxides by Two-Dimensional Correlation Spectroscopy. *Surf. Sci.* **2008**, *602*, 3637–3646. [[CrossRef](#)]

Disclaimer/Publisher's Note: The statements, opinions and data contained in all publications are solely those of the individual author(s) and contributor(s) and not of MDPI and/or the editor(s). MDPI and/or the editor(s) disclaim responsibility for any injury to people or property resulting from any ideas, methods, instructions or products referred to in the content.